Atmospheric Retrievals Suggest the Presence of a Secondary Atmosphere and Possible Sulfur Species on L98-59 d from JWST Nirspec G395H Transmission Spectroscopy

Agnibha Banerjee[1] , Joanna K. Barstow[1] , Amélie Gressier[2] , Néstor Espinoza[2] , David K. Sing[3] , Natalie H. Allen[3] ,
Stephan M. Birkmann[4] , Ryan C. Challener[5] , Nicolas Crouzet[6] , Carole A. Haswell[1] , Nikole K. Lewis[7] ,
Stephen R. Lewis[1] , and Jingxuan Yang[8]

[1] School of Physical Sciences, The Open University, Milton Keynes, MK7 6AA, UK; agnibha.banerjee@open.ac.uk
[2] Space Telescope Science Institute, 3700 San Martin Drive, Baltimore, MD 21218, USA
[3] William H. Miller III Department of Physics and Astronomy, Johns Hopkins University, Baltimore, MD 21218, USA
[4] European Space Agency, European Space Astronomy Centre, Camino Bajo del Castillo s/n, E-28692 Villanueva de la Cañada, Madrid, Spain
[5] Department of Astronomy, Cornell University, 122 Sciences Drive, Ithaca, NY 14853, USA
[6] Leiden Observatory, Leiden University, P.O. Box 9513, 2300 RA Leiden, The Netherlands
[7] Department of Astronomy and Carl Sagan Institute, Cornell University, 122 Sciences Drive, Ithaca, NY 14853, USA
[8] Atmospheric, Oceanic and Planetary Physics, Department of Physics, University of Oxford, Oxford, OX1 3PU, UK

Abstract

L 98-59 d is a Super-Earth planet orbiting an M-type star. We performed retrievals on the transmission spectrum of L 98-59 d obtained using NIRSpec G395H during a single transit, from JWST Cycle 1 GTO 1224. The wavelength range of this spectrum allows us to detect the presence of several atmospheric species. We found that the spectrum is consistent with a high mean molecular weight atmosphere. The atmospheric spectrum indicates the possible presence of the sulfur-bearing species H_2S and SO_2, which could hint at active volcanism on this planet if verified by future observations. We also tested for signs of stellar contamination in the spectrum and found signs of unocculted faculae on the star. The tentative signs of an atmosphere on L 98-59 d presented in this work from just one transit bodes well for possible molecular detections in the future, particularly as it is one of the best targets among small exoplanets for atmospheric characterization using JWST.

1. Introduction

The era of detection and characterization of atmospheres around rocky exoplanets is now here. E. M. May et al. (2023), J. Lustig-Yaeger et al. (2023), O. Lim et al. (2023), S. E. Moran et al. (2023), J. Kirk et al. (2024), and M. Damiano et al. (2024) have already used the immense capabilities of JWST to measure the transmission spectra of the atmospheres of rocky exoplanets. However, statistically significant detectable absorption features have been scarce—owing to the low atmospheric scale heights of rocky planets, possible cloud cover, and stellar contamination from the M-dwarf host stars (S. E. Moran et al. 2023).

Here, we conducted atmospheric retrievals on the transmission spectrum of L 98-59 d (R. Cloutier et al. 2019; V. B. Kostov et al. 2019). The L 98-59 system consists of two more rocky transiting planets and another nontransiting planet (O. D. S. Demangeon et al. 2021). Previous attempts to measure the transmission spectra between 1.1 and 1.7 μm of planet b (M. Damiano et al. 2022), planet c (T. Barclay et al. 2023), and planet d (L. Zhou et al. 2023) using Hubble Space Telescope WFC3 have not ruled out the possibility of high mean molecular weight or cloudy atmospheres. L. Zhou et al. (2023) ruled out cloud-free hydrogen and helium atmospheres for planets

c and d. However, they could not exclude the possibility of primary cloudy/hazy or water-rich atmospheres.

L 98-59 d is an ideal target for atmospheric studies due to its high transmission spectroscopy metric (E. M. R. Kempton et al. 2018) value. It may also sustain volcanism on its surface (D. Z. Seligman et al. 2024), providing a viable source for a secondary atmosphere or a mixed primary and secondary, or hybrid (M. Tian & K. Heng 2024) atmosphere.

L 98-59 d, with a radius of 1.52 $R_\oplus$, a mass of 1.94 $M_\oplus$, and an equilibrium temperature of 416 K, is inconsistent with a pure rocky (Earth-like) composition and is potentially too small to be explained by H-He gas accretion from the protoplanetary disk (R. Luque & E. Palle 2022). All three planets in the L 98-59 system receive substantial X-ray and extreme-ultraviolet flux, leading to rapid water loss that significantly affects their developing climates and atmospheres (E. F. Fromont et al. 2024). While there is no solid claim of an atmosphere on L 98-59 c, planet d is closer to the cosmic shoreline and more likely to possess an atmosphere. L 98-59 d's density categorizes it as a "water world" according to R. Luque & E. Palle (2022), suggesting a composition of rock and water ice in roughly equal proportions by mass. D. Z. Seligman et al. (2024) state that it may be possible to detect at atmosphere on L 98-59 d with 3–5 transits using NIRSpec/G395H, which could contain some amount of SO_2.

We analyzed a 2.9–5.2 μm JWST transmission spectrum obtained using NIRSpec (P. Ferruit et al. 2022; S. M. Birkmann et al. 2022), G395H. We performed several sets of atmospheric

retrievals with varying assumptions on this spectrum to infer the atmospheric composition of L 98-59 d. An atmospheric retrieval solves the inverse problem of going from a measured spectrum to the range of atmospheric properties consistent with the observations. This is done by comparing the observed spectrum with large numbers of generated spectra to explore the parameter space and finding the best-fitting combinations of model atmosphere properties (J. K. Barstow et al. 2017; A. Tsiaras et al. 2018; D. Grant et al. 2023; B. Benneke et al. 2024; M. Holmberg & N. Madhusudhan 2024; R. Hu et al. 2024; T. G. Beatty et al. 2024).

We used the transmission spectrum obtained for the JWST GTO 1224 program (PI: Birkmann) using NIRSpec G395H for one transit of L 98-59 d on 2023 June 25. The observations were reduced using two different pipelines—transitspectroscopy (N. Espinoza 2022) and FIREFLy (Z. Rustamkulov et al. 2022, 2023)—to obtain transmission spectra by binning the transit depths to a resolution of $R \sim 100$. The reduction methodology is discussed in detail in an accompanying paper from the GTO 1224 collaboration (A. Gressier et al. 2024), hereafter Paper I. The transitspectroscopy reduction is used for the majority of the retrievals in this Letter. For completeness, we also ran a retrieval on the FIREFLy reduction to explore the influence of data reduction on the retrieved parameters.

In Section 2 we describe the retrieval setup and the priors used for each parameter. In Section 3 we define the atmospheric models used for retrievals and discuss the results from the suite of retrievals that we have performed. In Section 4 we consider the significance of the presence of sulfur species in this atmosphere, compare results from the two independent data reductions presented in Paper I, and discuss the potential for future observations.

2. Methods

2.1. Retrieval Setup with NEMESISPY

Nonlinear optimal Estimator for Multivariate spectral analySIS (NEMESIS; P. G. J. Irwin et al. 2008) is a versatile retrieval tool widely employed in the study of planetary atmospheres, both within our solar system and beyond (J. K. Barstow et al. 2016; P. G. J. Irwin et al. 2018; A. S. Braude et al. 2020; J. K. Barstow 2020; P. G. J. Irwin et al. 2020, 2021; D. K. Sing et al. 2024). It utilizes a fast correlated-k method to solve the radiative transfer equation involving multiple absorbing gases. In this work, we used the Python adaptation of the Fortran-based NEMESIS, NEMESISPY (J. Yang et al. 2023, 2024a, 2024b).

We employed the PyMultiNest nested sampling solver (F. Feroz & M. P. Hobson 2008; F. Feroz et al. 2009; J. Buchner et al. 2014; F. Feroz et al. 2019) to explore potential solutions. Nested sampling (J. Skilling 2004, 2006) is a computational method for estimating the marginal likelihood of a model and performing Bayesian parameter estimation. It sequentially samples the prior distribution by generating live points and gradually fills the parameter space with points of increasing likelihood. In our study, we configured it with 2000 live points and an evidence tolerance value of 0.5.

For the gas opacities, we used k tables ($R = 1000$) from ExoMol (J. Tennyson et al. 2016; K. L. Chubb et al. 2021) encompassing the following molecular species: H_2O

(O. L. Polyansky et al. 2018), CO_2 (S. N. Yurchenko et al. 2020), CO (G. Li et al. 2015), NH_3 (P. A. Coles et al. 2019), PH_3 (C. Sousa-Silva et al. 2014), CH_4 (S. N. Yurchenko et al. 2017), SO_2 (D. S. Underwood et al. 2016), and H_2S (A. A. A. Azzam et al. 2016). These k tables are then channel-averaged to match the resolution of the data prior to the retrieval process (P. G. J. Irwin et al. 2020). We evaluate Rayleigh scattering cross sections using data from C. W. Allen (1976). Additionally, we incorporate collision-induced continuum absorption arising from H_2-H_2 (A. Borysow & L. Frommhold 1989; A. Borysow et al. 1989, 2001; A. Borysow 2002; L. S. Rothman et al. 2013), and N_2-N_2 (W. J. Lafferty et al. 1996).

2.2. Atmospheric Model

In our setup, the atmosphere was divided into 100 equal intervals in log-pressure, starting from 10^1 atm and extending to 10^{-7} atm. To remain agnostic of the atmosphere's background composition, we used centered log-ratio (CLR; B. Benneke & S. Seager 2012) priors for the gas abundances. The CLR parameterization treats all chemical species in the model equally, enabling any of them to be the dominant atmospheric species. This allows for a flexible exploration of possible background compositions. The CLR parameterization is a new addition to NEMESISPY, implemented in a manner similar to POSEIDON (R. J. MacDonald & N. Madhusudhan 2017; R. J. MacDonald 2023). Our implementation of CLR priors is nonuniform in the CLR space, and thus avoids biases in results, as described in M. Damiano & R. Hu (2021). In the log volume mixing ratio or log(VMR) space, this manifests as a distribution peaked in the high values and a flat tail toward the low values. We use 10^{-12} as the lower limit for the volume mixing ratios.

Clouds were represented using an opaque cloud top (P_{top}), with the prior for its logarithm, $\log(P_{top})$ defined as $\mathcal{U}(-7, 1)$ atm, and power-law scattering due to hazes above the cloud layer (R. J. MacDonald & N. Madhusudhan 2017), with the prior for power defined as $\mathcal{U}(-8, 4)$, where $\mathcal{U}(a, b)$ is a uniform distribution with a and b as the upper and lower bounds. We also include a Rayleigh enhancement parameter named Hazemult, with priors defined as $\mathcal{U}(-5, 5)$. We used an isothermal temperature–pressure profile, unless otherwise specified. The prior for the isothermal temperature was defined as $\mathcal{U}(311, 625)$ K. This choice is further explained in Section 2.3. The ratio of the radius of the planet at 10 atm to the white-light transit radius of the planet was left as a free parameter (f_{ref}) with the prior set as $\mathcal{U}(0.7, 1.3)$. Following L. Alderson et al. (2023) and E. M. May et al. (2023), we allowed for an offset between the NRS1 and NRS2 wavelength ranges. The prior distribution for this offset in ppm is set as $\mathcal{N}(0, 40)$, where $\mathcal{N}(\mu, \sigma)$ is a normal distribution with a mean of μ and a standard deviation of σ. The values of stellar effective temperature, stellar radius, and metallicity used were 3415 K, $0.303\,R_\odot$, and -0.46, respectively (O. D. S. Demangeon et al. 2021).

We represented stellar inhomogeneities using three parameters: fractional coverage f_{het}, the difference between photospheric temperature and heterogeneity temperature ΔT_{het}, and photospheric temperature T_{phot}. We followed the prescription used in POSEIDON (R. J. MacDonald & N. Madhusudhan 2017; A. D. Rathcke et al. 2021; R. J. MacDonald 2023), by using pysynphot (STScI Development Team 2013) to
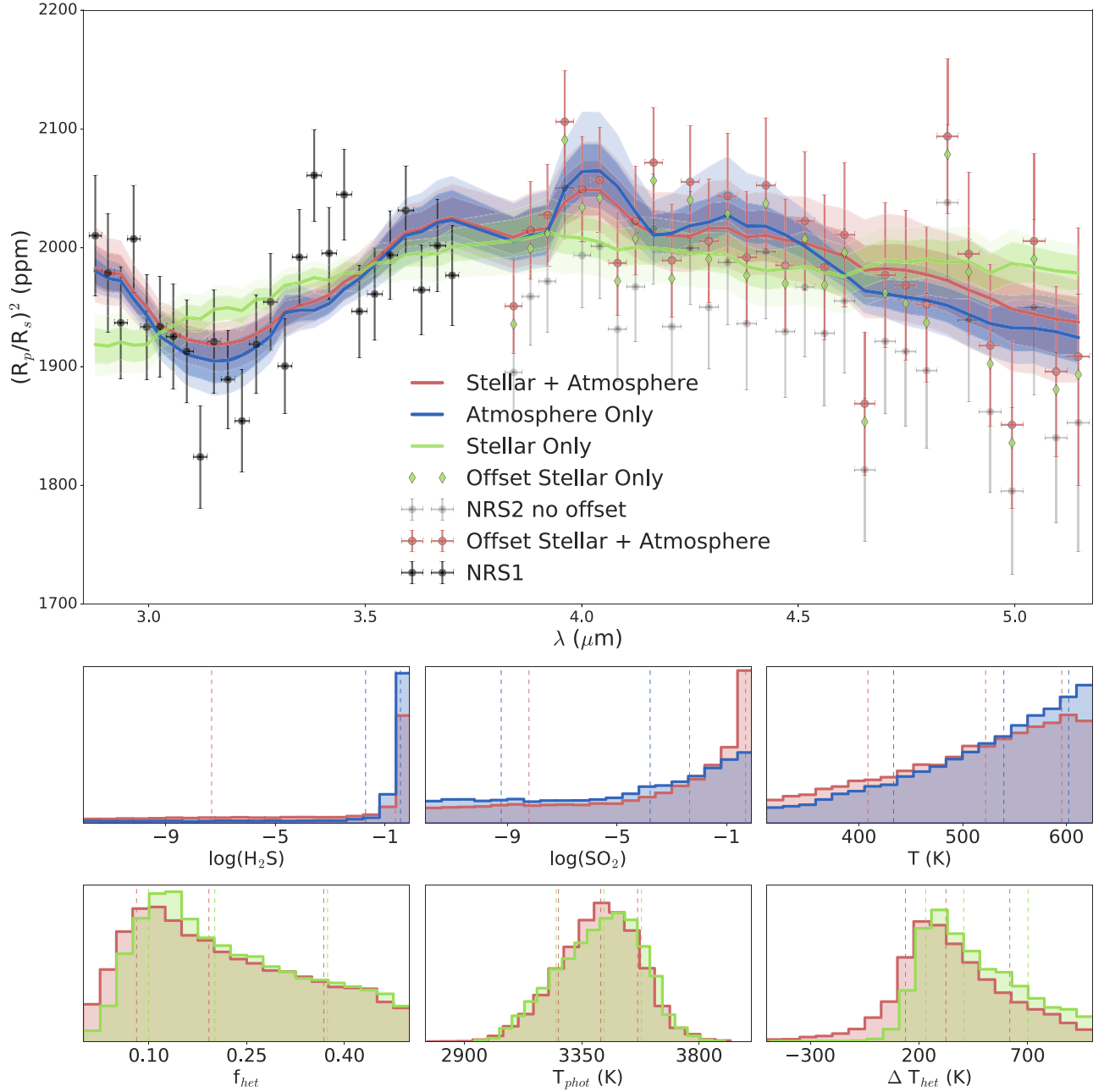
Figure 1. The retrieved spectra for the main retrievals: Stellar + Atmosphere scenario is plotted in red, Atmosphere Only in blue, and Stellar Only in green. The 1σ and 2σ credible intervals are plotted in dark and light shades of the corresponding colors, respectively. The NRS2 points are shifted by the retrieved offset, and the unshifted NRS2 points are shown in gray. Underneath the spectrum, in the first row from left to right, the retrieved posterior distributions for $\log(H_2S)$, $\log(SO_2)$, and temperature are shown. In the second row, from left to right, the retrieved posterior distributions for f_{het}, T_{phot}, and ΔT_{het} are shown.

sample a grid of PHOENIX (T. O. Husser et al. 2013) models, and representing unoccluded spots/faculae using stellar models with the same metallicity and $\log(g)$ values but a cooler/hotter temperature covering a fraction of the star.[9] The temperature of the heterogeneity is then defined as the sum of ΔT_{het} and T_{phot}. This is a simplified representation of stellar inhomogeneities and does not consider time-variable stellar activity. The priors for T_{phot}, ΔT_{het}, and f_{het} are defined as $\mathcal{N}(3415, 150)$ K, $\mathcal{U}(-500, 1000)$ K, and $\mathcal{U}(0, 0.5)$, respectively.

2.3. Constraining the Temperature

The magnitude of the features in a transmission spectrum is proportional to the vertical extent, and therefore the scale height, of the atmosphere. The scale height is directly proportional to atmospheric temperature and inversely proportional to the mean molecular weight of the atmosphere— creating a degeneracy between temperature and mean molecular weight. One way to mitigate this degeneracy is to specify physically motivated prior bounds on the temperature. Thus, we restricted the temperature priors to within 100 K of the theoretical limits of day-side temperature (T_d) of a planet considering both extremes of circulation, 411 K–525 K from N. B. Cowan & E. Agol (2011), giving a prior bound of 311 K–

---

[9] `pysynphot` has a known issue with interpolating PHOENIX spectra for some stellar metallicities and temperatures. We find no evidence of the issue for the values of metallicity and temperature that we use.

Table 1
Priors and Retrieved Values of Atmospheric Parameters from a Selection of Retrievals

	Priors	Posteriors					
		Main Retrievals			Alternate Retrievals		
		Stellar + Atmosphere	Atmosphere Only	Stellar Only	Equilibrium	No H_2S/SO_2	FIREFLy
$\log(H_2S)$	CLR	$-0.62^{+0.61}_{-6.73}$	$-0.44^{+0.42}_{-1.30}$	...	...	...	$-4.07^{+3.93}_{-5.11}$
$\log(SO_2)$	CLR	$-2.35^{+2.05}_{-5.88}$	$-3.79^{+2.90}_{-5.45}$	...	...	...	$-2.04^{+1.94}_{-6.03}$
$\log(H_2O)$	CLR	<-0.3	<-2.7	...	...	$-5.26^{+4.33}_{-4.33}$	<-0.1
$\log(CO_2)$	CLR	<-0.4	<-1.8	...	...	$-4.88^{+4.41}_{63}$	<-0.1
$\log(CO)$	CLR	<-0.3	<-0.9	...	...	$-5.22^{+4.43}_{-4.38}$	<-0.1
$\log(NH_3)$	CLR	<-1.6	<-4.8	...	...	$-5.87^{+4.14}_{-4.00}$	<-0.4
$\log(PH_3)$	CLR	<-0.4	<-4.0	...	...	$-1.70^{+1.69}_{-6.27}$	<-0.1
$\log(CH_4)$	CLR	<-1.8	<-4.4	...	...	$-6.02^{+4.10}_{-3.85}$	<-0.9
$\log(N_2)$	CLR	$-5.25^{+4.43}_{-4.40}$	$-5.53^{+4.38}_{-4.31}$	...	...	$-4.76^{+4.34}_{-4.61}$	$-5.21^{+4.40}_{-4.42}$
T (K)	$\mathcal{U}(311, 625)$	522^{+73}_{-113}	539^{+62}_{-106}	...	467^{+108}_{-99}	458^{+94}_{-97}	486^{+94}_{-110}
$\log(P_{top}/\mathrm{atm})$	$\mathcal{U}(-7, 1)$	$-0.65^{+1.11}_{-2.08}$	$-0.12^{+0.77}_{-0.98}$	...	$-1.28^{+1.48}_{-2.02}$	$-2.80^{+2.41}_{-2.43}$	$-1.73^{+1.84}_{-2.67}$
Power	$\mathcal{U}(-8, 4)$	$-2.28^{+4.08}_{-3.80}$	$-1.78^{+3.88}_{-4.18}$	...	$-2.32^{+4.10}_{-3.61}$	$-2.62^{+4.02}_{-3.57}$	$-2.35^{+4.08}_{-3.67}$
Hazemult	$\mathcal{U}(-5, 5)$	$-2.13^{+2.75}_{-1.87}$	$-2.82^{+1.66}_{-1.47}$	...	$-1.59^{+2.73}_{-2.23}$	$0.64^{+2.96}_{-3.57}$	$-0.98^{+3.29}_{-2.67}$
f_{ref}	$\mathcal{U}(0.7, 1.3)$	$0.97^{+0.01}_{-0.02}$	$0.94^{+0.01}_{-0.01}$	$0.99^{+0.01}_{-0.01}$	$0.94^{+0.01}_{-0.01}$	$0.97^{+0.01}_{-0.02}$	$0.98^{+0.01}_{-0.01}$
Offset (ppm)	$\mathcal{N}(0, 40)$	$47.24^{+20.35}_{-18.57}$	$26.16^{+16.04}_{-15.29}$	$45.23^{+17.60}_{-18.15}$	$6.86^{+15.07}_{-14.51}$	$55.48^{+23.40}_{-22.26}$	$15.27^{+20.34}_{-20.14}$
f_{het}	$\mathcal{U}(0, 0.5)$	$-0.19^{+0.18}_{-0.11}$	...	$0.20^{+0.17}_{-0.10}$	...	$0.24^{+0.16}_{-0.12}$	$0.23^{+0.16}_{-0.11}$
T_{phot}	$\mathcal{N}(3415, 150)$	3423^{+141}_{-162}	...	3435^{+144}_{-183}	...	3422^{+136}_{-177}	3397^{+152}_{-166}
ΔT_{het}	$\mathcal{U}(-500, 1000)$	324^{+295}_{-187}	...	406^{+297}_{-175}	...	403^{+264}_{-147}	426^{+277}_{-164}
$Z/Z_{\odot}$	$\mathcal{U}(0.1, 1000)$	...	...	...	533^{+257}_{-226}	...	...
C/O	$\mathcal{U}(0.1, 2.0)$	...	...	...	$0.58^{+0.49}_{-0.28}$	...	...
S/O	$\mathcal{U}(0.1, 2.0)$	...	...	...	$1.16^{+0.55}_{-0.61}$	...	...
$\ln(Z)$		462.92	462.07	461.54	459.93	461.39	471.30
Number of parameters		18	15	5	9	16	18
MMW (amu)		10.36	11.07	...	32.14	27.22	30.02
χ^2_{red}		1.56	1.44	1.73	1.78	1.98	1.51
σ		2.24	1.70	Baseline	Not preferred	Not preferred	1.67

Note. Only 2σ upper bounds are specified for the gas abundances that are not constrained. The detection significance σ is computed by comparing the Bayesian log evidence of each model with the Stellar Only case for each reduction. For the FIREFLy retrieval, the baseline Stellar Only $\ln(Z)$ is 470.80.

625 K.

$$T_{d} = T_0(1 - A_B)^{1/4}\left(\frac{2}{3} - \frac{5}{12}\varepsilon\right)^{1/4}, \qquad (1)$$

where ε denotes the circulation efficiency from 0 to 1, A_B is the planetary albedo, and T_0 is

$$T_0 = T_*\left(\frac{R_*}{a}\right)^{1/2}, \qquad (2)$$

where T_* is the stellar effective temperature, R_* is the stellar radius, and a is the star–planet distance. The day-side temperature is used as a conservative estimate, as the terminator temperature that we are sensitive to in transmission spectroscopy should be lower than that.

3. Atmospheric Retrievals

3.1. Main Retrievals

As transmission spectra of planets around M-dwarfs have been plagued by stellar contamination (O. Lim et al. 2023; S. E. Moran et al. 2023), for our main retrieval, we included stellar contamination. As no evidence of spot crossings was seen in the light curves, here we only modeled unocculted inhomogeneites. As an additional test, we checked whether a scenario with a planetary atmosphere but no stellar

inhomogeneities can reproduce the spectrum. For this case, the priors for the parameters related to the planet's atmospheres were kept the same, but the stellar parameters were removed.

We verified whether a bare rock planet can still produce this spectrum if stellar inhomogeneities are present. For this scenario, we modeled the planet's contribution using only two parameters: the reference radius and the offset between NRS1 and NRS2. The priors for the stellar contribution parameters were left unchanged. We also tried a similar scenario with the planet's contribution only, essentially checking if a flat line with an offset between NRS1 and NRS2 can explain the spectrum. For each of our retrievals, we calculated a Bayesian log-evidence value and compared it to this case. The values of sigma are computed using the difference in log evidence (R. Trotta 2008; B. Benneke & S. Seager 2013).

3.2. Results from Main Retrievals

The main retrieval with stellar inhomogeneities and a planetary atmosphere favors an atmosphere with high H_2S and SO_2 abundances, with log(VMR) of $-0.62^{+0.61}_{-6.73}$ and $-2.35^{+2.05}_{-5.88}$, respectively. It also suggests the presence of unoccluted stellar faculae, as ΔT_{het} is positive with a retrieved value of 324^{+295}_{-187} K. The retrieved models and selected posterior distributions for some parameters are shown in Figure 1. The
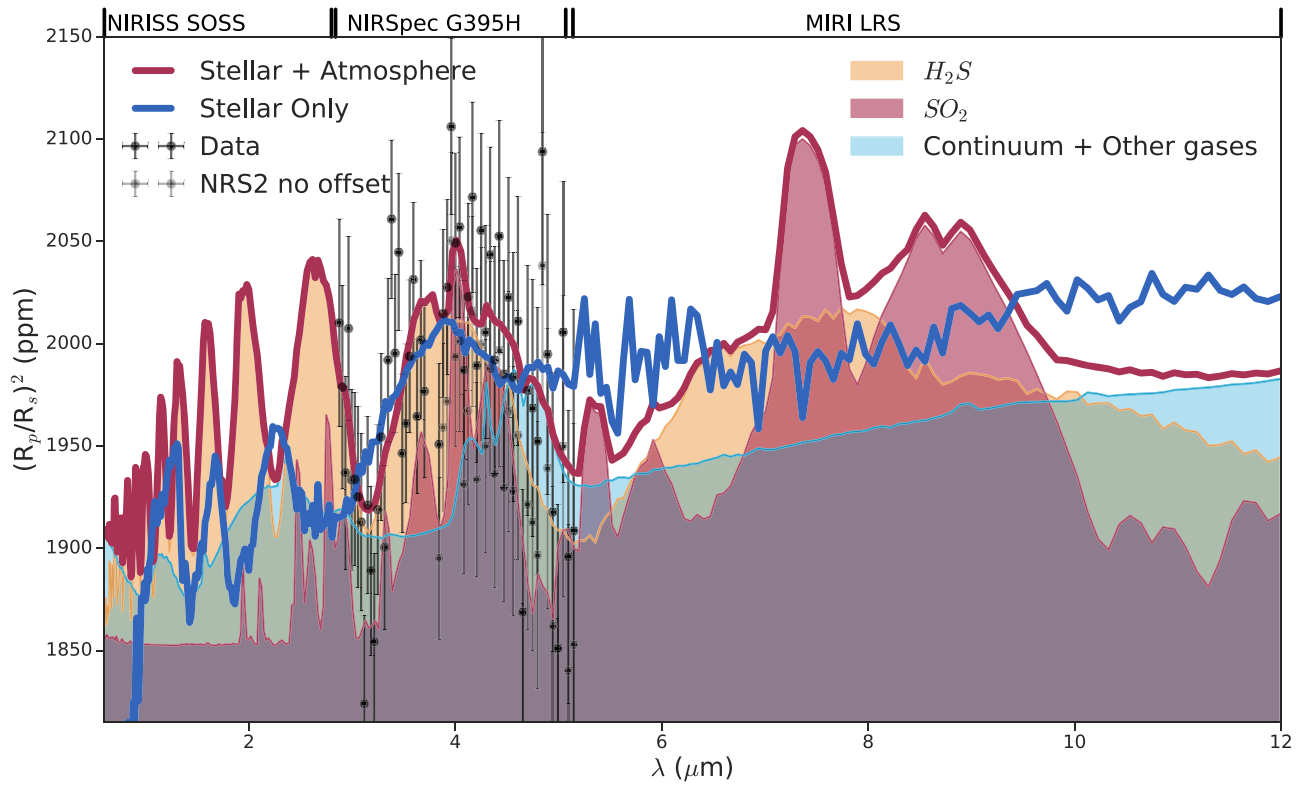
Figure 2. This plot shows the retrieved spectra from the main retrieval scenarios of stellar inhomogeneities with planetary atmospheres and stellar inhomogeneities only extended to the 0.6–12 μm JWST wavelength range. The gas contributions for H_2S and SO_2 are highlighted. The available wavelength ranges for different JWST instruments are marked at the top of the plot. Several H_2S features in the NIRISS SOSS range, combined H_2S and SO_2 features in the NIRSpec G395H range, and SO_2 features in the MIRI LRS range may be detectable in future observations.

best-fit model extended to between 0.6 and 12 μm is shown in Figure 2. The full corner plot is shown in Figure 3. The results from all of the retrievals are listed in Table 1.

The retrieval with only stellar inhomogeneities failed to provide a good fit to the observed spectrum but resulted in similar posteriors for the stellar parameters. It is worth noting that this scenario fails to reproduce the feature at about 4 μm, which can be attributed to SO_2. This confirms the results of Paper I that stellar activity alone cannot reproduce the observed spectrum. The scenario with the planet's contribution only (the flat line with an offset) provided a much worse fit to the spectrum—resulting in a reduced chi-squared value of only 1.86.

The fit with stellar inhomogeneities and an atmosphere was preferred at 2.24σ to the fit with only stellar inhomogeneities, and at 3.50σ to the fit with only a flat line and offset. The fit with only a planetary atmosphere also favors an atmosphere with high abundances of H_2S and SO_2.

The individual detection significances of H_2S and SO_2, calculated by removing each gas in turn from the main retrieval with stellar inhomogeneities and planetary atmosphere are about 2σ. Thus, these can only be interpreted as weak detections.

3.3. Alternate Retrieval Setups

In addition to the main retrievals, we also considered some alternate retrieval setups to test whether our choice of parameterization affects the inferences. The representation and priors for all parameters are as described in Section 2.2, unless otherwise stated.

3.3.1. Equilibrium Chemistry Retrieval

We performed a retrieval enforcing equilibrium chemistry using NEMESISPY (J. Yang et al. 2023, 2024a, 2024b), coupled with the FastChem (J. W. Stock et al. 2018; J. W. Stock & D. Kitzmann 2022) chemical solver. We parameterized elemental abundances using three parameters: metallicity ($Z/Z_\odot$), carbon-to-oxygen ratio (C/O), and sulfur-to-oxygen ratio (S/O). The prior distributions for these parameters were set as $\mathcal{U}(0.1, 1000)$, $\mathcal{U}(0.1, 2.0)$, and $\mathcal{U}(0.1, 2.0)$, respectively. This retrieval struggled to produce a good fit to the data and was not preferred to the baseline model of having only stellar inhomogeneities. This indicates that the atmosphere is probably not in equilibrium. The retrieved model and selected posterior distributions for some parameters are shown in Figure 4.

3.3.2. No H_2S/SO_2

In an alternate version of the main retrieval, we removed H_2S and SO_2 from the active gases. This retrieval also struggled to produce a good fit to the data and was not preferred to the baseline model having only stellar inhomogeneities. This result is further evidence of the tentative presence of these sulfur species in the atmosphere. The retrieved model and selected posterior distributions for some parameters are shown in Figure 4.

3.3.3. Nitrogen Background

In another alternate version of the main retrieval, we assumed that the planet has a nitrogen-dominated atmosphere

as nitrogen is another gas that only has continuum features in this wavelength range. Thus, we fixed the background to N_2, and used log-uniform priors for the trace gases, with priors for log(VMR) set to $\mathcal{U}(-12, -0.1)$. This also resulted in significant H_2S and SO_2 abundances. This indicates that the choice of CLR priors does not bias our inferences of the atmosphere.

3.3.4. Temperature–Pressure Retrieval

In this alternate version of the main retrieval, we tested the application of a nonisothermal temperature–pressure profile using the parameterization of N. Madhusudhan & S. Seager (2009). We found that this made a negligible difference to the quality of the fit, and the retrieved profile was close to isothermal, indicating that a nonisothermal profile is not statistically favored for this spectrum. This is probably because the spectrum probes a relatively narrow pressure range. This retrieval also resulted in high H_2S and SO_2 abundances.

We have also performed retrievals in which the isothermal temperature was allowed to vary between 100 K and 1000 K. In these, the retrieved temperatures were either much higher than the calculated bounds, when the atmospheric mean molecular weight was high, or much lower, for a low mean molecular weight atmosphere. The actual solution could possibly lie in between these extremes, and without informative prior bounds, the molecular weight and temperature are highly degenerate. These retrievals also recovered high H_2S and SO_2 abundances. Thus, this degeneracy does not affect the possible presence of sulfur species, which is discussed in Section 4.1.

4. Discussion

4.1. Possible Presence of Sulfur Species

The primary contributors to the retrieved spectrum across all the retrieval setups we tested are invariably H_2S and SO_2, which are both prominent sulfur species. To test their significance, we removed them from the list of active species and performed another retrieval, otherwise identical to the main retrieval as described in Section 3.3.2. This produced a much worse fit to the spectrum than the model with the sulfur species. By comparing the log evidence for these two scenarios, we obtain a combined detection significance of 2.32σ for H_2S and SO_2.

Previous studies have suggested that L 98-59 d is a planet that is being tidally heated (D. Z. Seligman et al. 2024). It has a nonzero eccentricity of $0.074^{+0.057}_{-0.046}$ (O. D. S. Demangeon et al. 2021) and the planets b, c, and d have orbital resonances close to 2:4:7 (D. Z. Seligman et al. 2024). Tidal stresses could lead to volcanic outgassing, similar to the volcanic activity on Jupiter's moon Io, and could be a possible source of H_2S and SO_2 in the atmosphere. Recent modeling studies have also suggested volcanic or outgassed origins of H_2S and SO_2 (A. B. Claringbold et al. 2023; S.-M. Tsai et al. 2024) in exoplanet atmospheres.

We find that the abundances of common atmospheric species such as H_2O and CO_2 are unconstrained with long tails in the posterior distribution, and we only report upper bounds for their abundances. The possible presence of H_2S also supports the absence of CO_2 and H_2O, as H_2S features in the spectrum would not be visible if they were present (L. J. Janssen et al. 2023). As H_2O is required in the photochemical production of SO_2, as shown in S.-M. Tsai et al. (2023), photochemistry is

unlikely to be the source of SO_2 in the atmosphere of L 98-59 d. While the possible presence of H_2S and SO_2 in the absence of H_2O and CO_2 is unlikely in equilibrium conditions (L. J. Janssen et al. 2023), they might exist on an intensely volcanic planet.

We also do not detect the presence of any significant clouds or haze scattering. If H_2S and SO_2 are present, S. Jordan et al. (2021) found that these should survive above the cloud layer in the atmospheres of planets around M-dwarfs, where they could be detectable.

4.2. Comparison between Reductions

L 98-59 d has a high impact parameter (O. D. S. Demangeon et al. 2021) and the transit chord crosses near to the limb of the host star from our perspective, thus making it difficult to pin down the limb darkening coefficients Paper I.

To check the effect of data reduction methods on our retrievals, we performed all the same retrievals on another reduction of the spectrum using FIREFLy. Here, we present a retrieval identical to our main retrieval, using this reduction instead. While there are some differences in the retrieved parameters, the high H_2S and SO_2 abundances are still present —with log(VMR) of $-4.07^{+3.93}_{-5.11}$ and $-2.04^{+1.94}_{-6.03}$, respectively. We performed a fit with a baseline stellar inhomogeneities only for this reduction as well. This atmospheric model is preferred at 1.67σ to the equivalent baseline fit. The retrieved model and selected posterior distributions are shown in Figure 5.

4.3. Comparison between Retrieval Codes

Previous studies have compared the results obtained using different retrieval codes for the same spectrum (J. K. Barstow et al. 2020; J. Taylor et al. 2023). Subtle differences in the forward models used to perform retrievals can lead to significant differences in retrieved parameters. To test if our inferences are being impacted by the choice of retrieval codes, we performed a retrieval with a similar setup as our main retrieval using Taurex3 (A. F. Al-Refaie et al. 2021). This retrieval, presented in Paper I, also produced similarly high abundances of H_2S and SO_2.

4.4. Future Observations

Figure 2 shows the best-fit model extended to between 0.6 and 12 μm. This shows H_2S and SO_2 features in other regions of the spectrum, accessible to JWST instruments NIRISS, NIRSpec, and MIRI. Observations in the 0.6–5.0 μm range can possibly confirm or refute the signatures of these sulfur species. An accepted JWST proposal in Cycle 1: GTO 1201 (PI: Lafreniere) includes one transit of L 98-59 d with NIRISS SOSS. An accepted JWST proposal in Cycle 2: GO 4098 (PI: Benneke) also includes one transit of L 98-59 d with NIRSpec G395H and one transit with NIRISS SOSS. Apart from these, MIRI observations can particularly help pin down the large SO_2 features in the 7–10 μm range.

5. Conclusion

We have presented a range of retrieval analyses for the NIRSpec/G395H spectrum of L 98-59 d. Our analyses favor an atmosphere with substantial amounts of sulfur species H_2S and SO_2, and an atmospheric temperature higher than the equilibrium temperature. We also find evidence of unocculted

faculae on the star. The rocky planets in the solar system all have different atmospheric compositions, and the study of such atmospheres in exoplanetary systems could unlock a rich diversity of unexplored chemistries.

Our retrievals do not constrain the abundances of other spectrally active gases such as H_2O and CO_2, and we only report upper bounds. The bare rock with stellar inhomogeneities scenario struggles to reproduce the observed spectral features. Several H_2S and SO_2 features exist in other wavelength regions covered by JWST, as shown in Figure 2. The two scenarios of stellar inhomogeneity with an atmosphere and only stellar inhomogeneity also differ in other wavelength regions. Follow-up observations in these wavelengths can confirm or refute the evidence of H_2S and SO_2, and distinguish between a planetary atmosphere and stellar inhomogeneities.

Appendix A
Corner plot

Here, in Figure 3, we show the full corner plot for the main retrieval including stellar inhomogeneities and a planetary atmosphere. The full corner plots for all the retrievals mentioned in this Letter can be found at:https://github.com/riobanerjee/supplement_L9859d.
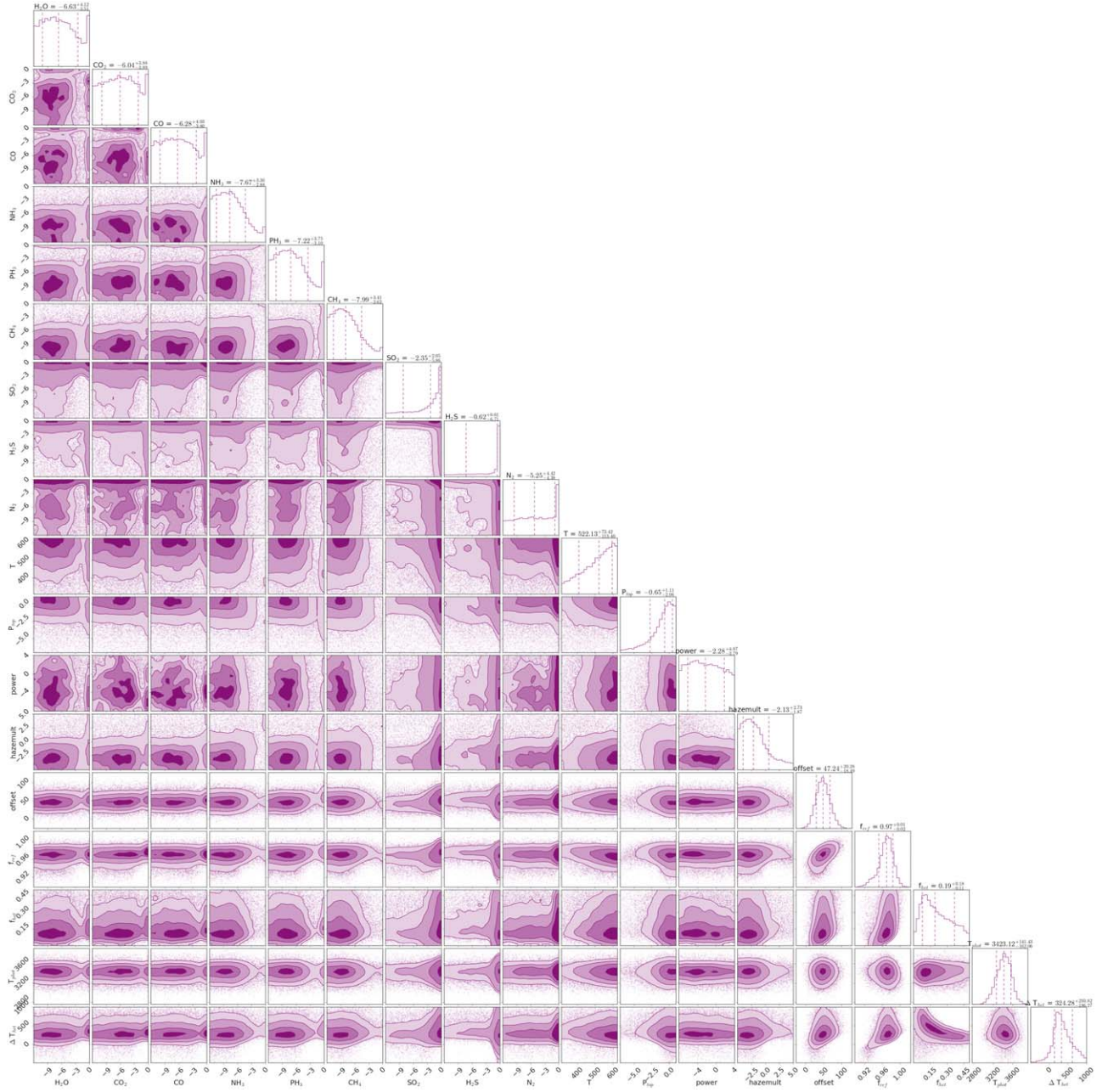
Figure 3. The corner plot showing retrieved posterior distributions for each parameter for the main retrieval. The plots on the diagonal show the histograms of retrieved parameters and the inner plots show the pairwise correlations between the parameters. Large abundances for H_2S and SO_2 can be seen, with upper bounds for all other active gases.

Appendix B
Alternate Retrieval Plot

Here, in Figure 4, we show the spectral fits and posteriors for selected parameters for two of the alternate retrievals: equilibrium chemistry and the retrieval without H_2S and SO_2 included.
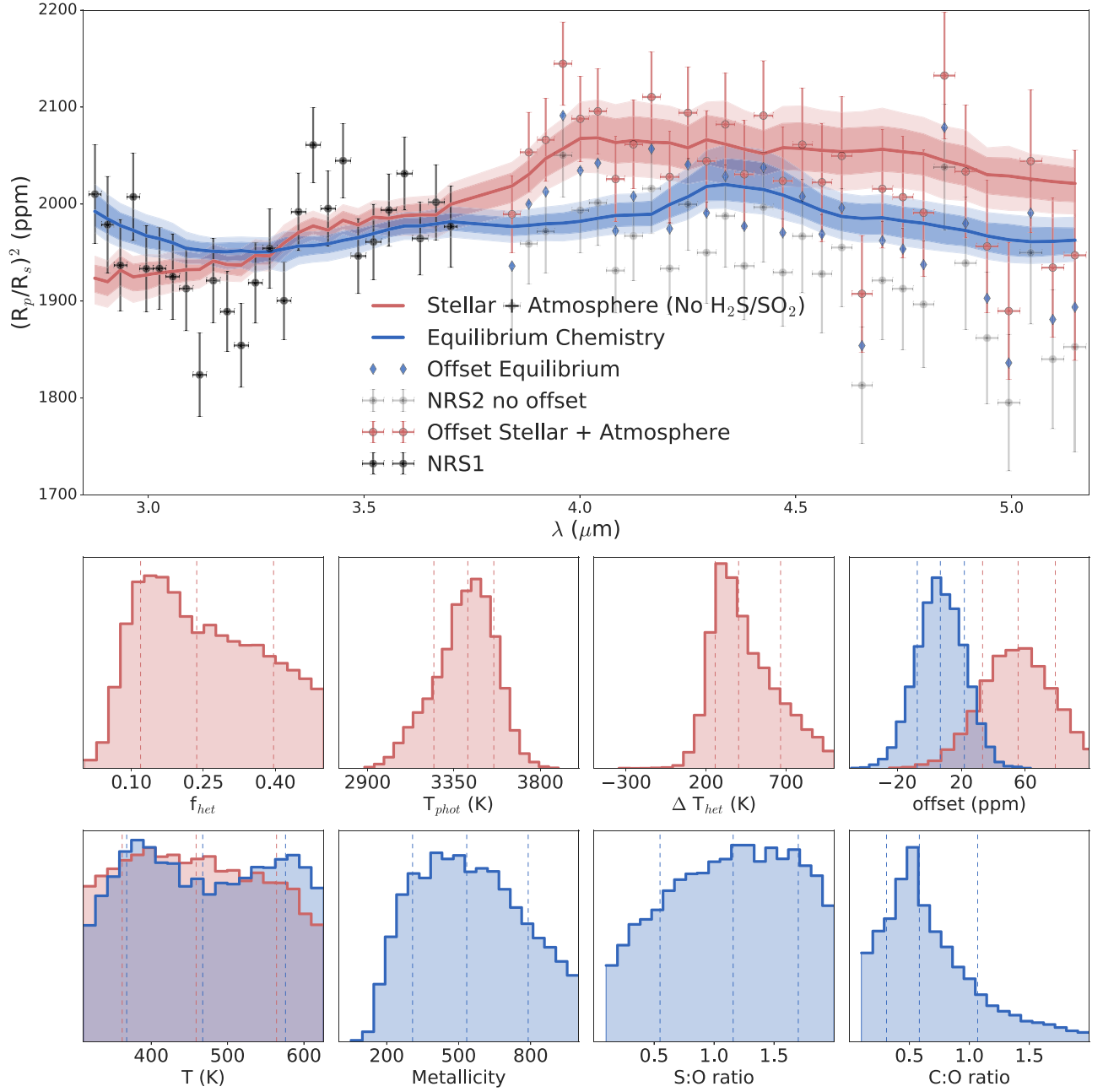
Figure 4. The retrieved spectra for the two alternate retrievals are shown: the Stellar + Atmosphere scenario with H_2S and SO_2 removed is plotted in red and the equilibrium chemistry scenario is plotted in blue. The 1σ and 2σ credible intervals are plotted in dark and light shades of the corresponding colors, respectively. The NRS2 points are shifted by the retrieved offset, and the unshifted NRS2 points are shown in gray. Underneath the spectrum, in the first row from left to right, the retrieved posterior distributions for f_{het}, T_{phot}, ΔT_{het}, and offset are shown. In the second row, from left to right, the retrieved posterior distribution for temperature, metallicity, S:O ratio, and C:O ratio are shown.

Appendix C
Comparison between Reductions Plot

Here, in Figure 5, we show the spectral fits and posteriors for selected parameters for retrievals using two different reductions: `transitspectroscopy` and `FIREFLy`.
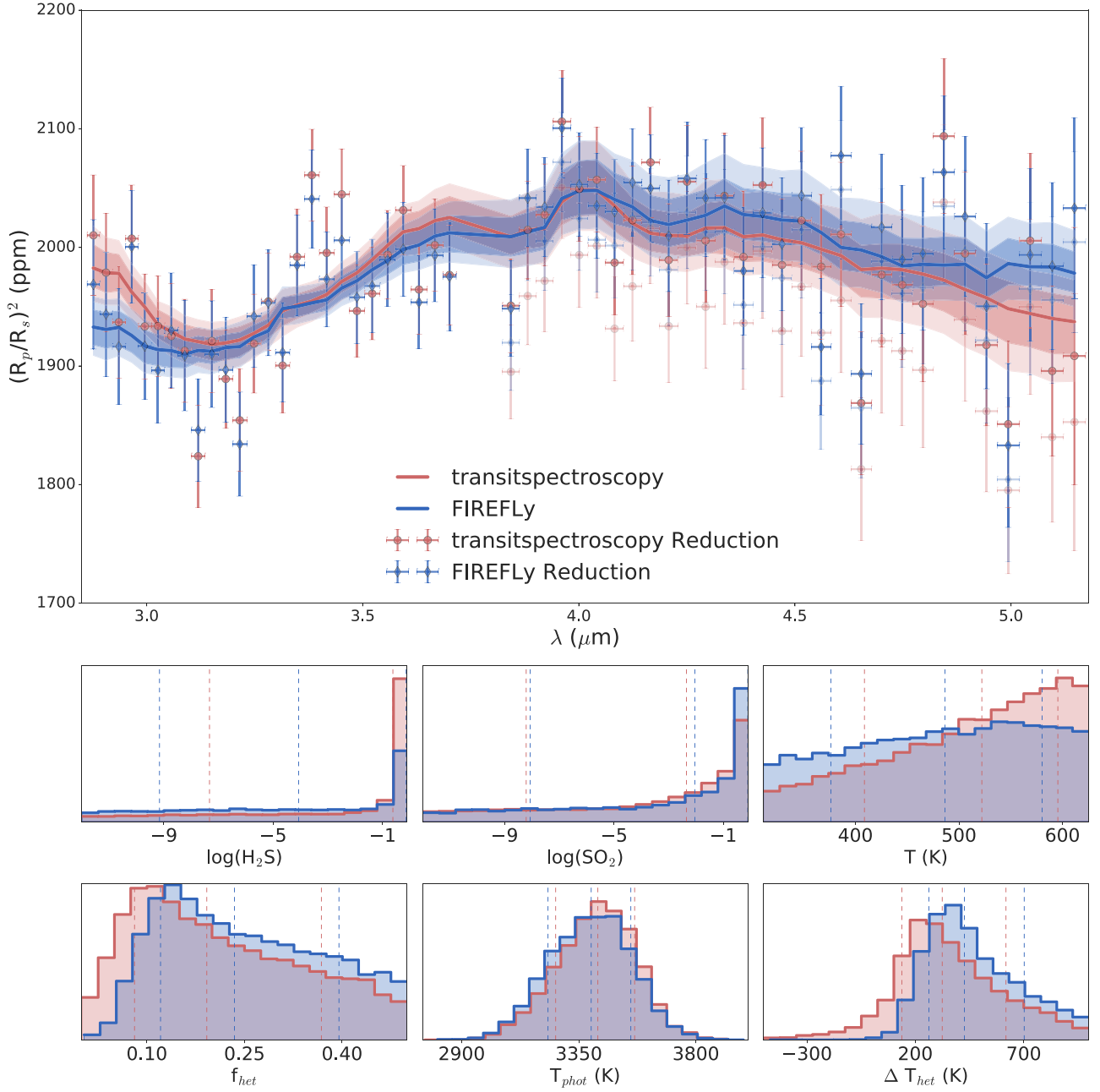
Figure 5. The retrieved spectra for the retrievals using two different reductions are shown: `transitspectroscopy` is plotted in red and `FIREFLy` is plotted in blue. The 1σ and 2σ credible intervals are plotted in dark and light shades of the corresponding colors, respectively. The NRS2 points are shifted by the retrieved offset, and the unshifted NRS2 points are shown in gray. Underneath the spectrum, in the first row from left to right, the retrieved posterior distributions for $\log(H_2S)$, $\log(SO_2)$, and temperature are shown. In the second row, from left to right, the retrieved posterior distributions for f_{het}, T_{phot}, and ΔT_{het} are shown.

ORCID iDs

Agnibha Banerjee ⦿ https://orcid.org/0000-0002-9124-6537
Joanna K. Barstow ⦿ https://orcid.org/0000-0003-3726-5419
Amélie Gressier ⦿ https://orcid.org/0000-0003-0854-3002
Néstor Espinoza ⦿ https://orcid.org/0000-0001-9513-1449
David K. Sing ⦿ https://orcid.org/0000-0001-6050-7645
Natalie H. Allen ⦿ https://orcid.org/0000-0002-0832-710X
Stephan M. Birkmann ⦿ https://orcid.org/0000-0001-7058-1726
Ryan C. Challener ⦿ https://orcid.org/0000-0002-8211-6538
Nicolas Crouzet ⦿ https://orcid.org/0000-0001-7866-8738
Carole A. Haswell ⦿ https://orcid.org/0000-0002-8050-1897

Nikole K. Lewis ⦿ https://orcid.org/0000-0002-8507-1304
Stephen R. Lewis ⦿ https://orcid.org/0000-0001-7237-6494
Jingxuan Yang ⦿ https://orcid.org/0009-0006-2395-6197

References

Al-Refaie, A. F., Changeat, Q., Waldmann, I. P., & Tinetti, G. 2021, ApJ, 917, 37
Alderson, L., Wakeford, H. R., Alam, M. K., et al. 2023, Natur, 614, 664
Allen, C. W. 1976, Astrophysical Quantities (London: Athlone)
Azzam, A. A. A., Tennyson, J., Yurchenko, S. N., & Naumenko, O. V. 2016, MNRAS, 460, 4063
Barclay, T., Sheppard, K. B., Latouf, N., et al. 2023, arXiv:2301.10866
Barstow, J. K. 2020, MNRAS, 497, 4183

Barstow, J. K., Aigrain, S., Irwin, P. G. J., Kendrew, S., & Fletcher, L. N. 2016, MNRAS, 458, 2657
Barstow, J. K., Aigrain, S., Irwin, P. G. J., & Sing, D. K. 2017, ApJ, 834, 50
Barstow, J. K., Changeat, Q., Garland, R., et al. 2020, MNRAS
Beatty, T. G., Welbanks, L., Schlawin, E., et al. 2024, ApJL, 970, L10
Benneke, B., & Seager, S. 2012, ApJ, 753, 100
Benneke, Björn, & Seager, Sara 2013, ApJ, 778, 153
Benneke, B., Roy, P.-A., Coulombe, L.-P., et al. 2024, arXiv:2403.03325
Birkmann, S. M., Ferruit, P., Giardino, G., et al. 2022, A&A, 661, A83
Borysow, A. 2002, A&A, 390, 779
Borysow, A., & Frommhold, L. 1989, ApJ, 341, 549
Borysow, A., Frommhold, L., & Moraldi, M. 1989, ApJ, 336, 495
Borysow, A., Jorgensen, U. G., & Fu, Y. 2001, JQSRT, 68, 235
Braude, A. S., Irwin, P. G. J., Orton, G. S., & Fletcher, L. N. 2020, Icar, 338, 113589
Buchner, J., Georgakakis, A., Nandra, K., et al. 2014, A&A, 564, A125
Chubb, K. L., Rocchetto, M., Yurchenko, S. N., et al. 2021, A&A, 646, A21
Claringbold, A. B., Rimmer, P. B., Rugheimer, S., & Shorttle, O. 2023, AJ, 166, 39
Cloutier, R., Astudillo-Defru, N., Doyon, R., et al. 2019, A&A, 621, A49
Coles, P. A., Yurchenko, S. N., & Tennyson, J. 2019, MNRAS, 490, 4638
Cowan, N. B., & Agol, E. 2011, ApJ, 729, 54
Damiano, M., Bello-Arufe, A., Yang, J., & Hu, R. 2024, ApJL, 968, L22
Damiano, M., & Hu, R. 2021, AJ, 162, 200
Damiano, M., Hu, R., Barclay, T., et al. 2022, AJ, 164, 225
Demangeon, O. D. S., Zapatero Osorio, M. R., Alibert, Y., et al. 2021, A&A, 653, A41
Espinoza, N. 2022, TransitSpectroscopy, v0.3.11, Zenodo, doi:10.5281/zenodo.6960924
Feroz, F., & Hobson, M. P. 2008, MNRAS, 384, 449
Feroz, F., Hobson, M. P., & Bridges, M. 2009, MNRAS, 398, 1601
Feroz, F., Hobson, M. P., Cameron, E., & Pettitt, A. N. 2019, OJAp, 2, 10
Ferruit, P., Jakobsen, P., Giardino, G., et al. 2022, A&A, 661, A81
Fromont, E. F., Ahlers, J. P., do Amaral, L. N. R., et al. 2024, ApJ, 961, 115
Grant, D., Lewis, N. K., Wakeford, H. R., et al. 2023, ApJ, 956, L32
Gressier, A., Espinoza, N., Allen, N. H., et al. 2024, arXiv:2408.15855
Holmberg, M., & Madhusudhan, N. 2024, A&A, 683, L2
Hu, R., Bello-Arufe, A., Zhang, M., et al. 2024, Natur, 630, 609
Husser, T. O., Wende-von Berg, S., Dreizler, S., et al. 2013, A&A, 553, A6
Irwin, P. G. J., Dobinson, J., James, A., et al. 2021, Icar, 357, 114277
Irwin, P. G. J., Parmentier, V., Taylor, J., et al. 2020, MNRAS, 493, 106
Irwin, P. G. J., Teanby, N. A., de Kok, R., et al. 2008, JQSRT, 109, 1136
Irwin, P. G. J., Toledo, D., Garland, R., et al. 2018, NatAs, 2, 420
Janssen, L. J., Woitke, P., Herbort, O., et al. 2023, AN, 344, e20230075
Jordan, S., Rimmer, P. B., Shorttle, O., & Constantinou, T. 2021, ApJ, 922, 44
Kempton, E. M. R., Bean, J. L., Louie, D. R., et al. 2018, PASP, 130, 114401
Kirk, J., Stevenson, K. B., Fu, G., et al. 2024, AJ, 167, 90
Kostov, V. B., Schlieder, J. E., Barclay, T., et al. 2019, AJ, 158, 32

Lafferty, W. J., Solodov, A. M., Weber, A., Olson, W. B., & Hartmann, J.-M. 1996, ApOpt, 35, 5911
Li, G., Gordon, I. E., Rothman, L. S., et al. 2015, ApJS, 216, 15
Lim, O., Benneke, B., Doyon, R., et al. 2023, ApJL, 955, L22
Luque, R., & Palle, E. 2022, Sci, 377, 1211
Lustig-Yaeger, J., Fu, G., May, E. M., et al. 2023, NatAs, 7, 1317
MacDonald, R. J. 2023, JOSS, 8, 4873
MacDonald, R. J., & Madhusudhan, N. 2017, MNRAS, 469, 1979
Madhusudhan, N., & Seager, S. 2009, ApJ, 707, 24
May, E. M., MacDonald, R. J., Bennett, K. A., et al. 2023, ApJL, 959, L9
Moran, S. E., Stevenson, K. B., Sing, D. K., et al. 2023, ApJL, 948, L11
Polyansky, O. L., Kyuberis, A. A., Zobov, N. F., et al. 2018, MNRAS, 480, 2597
Rathcke, A. D., MacDonald, R. J., Barstow, J. K., et al. 2021, AJ, 162, 138
Rothman, L. S., Gordon, I. E., Babikov, Y., et al. 2013, JQSRT, 130, 4
Rustamkulov, Z., Sing, D. K., Liu, R., & Wang, A. 2022, ApJL, 928, L7
Rustamkulov, Z., Sing, D. K., Mukherjee, S., et al. 2023, Natur, 614, 659
Seligman, D. Z., Feinstein, A. D., Lai, D., et al. 2024, ApJ, 961, 22
Sing, D. K., Rustamkulov, Z., Thorngren, D. P., et al. 2024, Natur, 630, 831
Skilling, J. 2004, in AIP Conference Proceedings, 735 (Melville, NY: AIP), 395
Skilling, J. 2006, BayAn, 1, 833
Sousa-Silva, C., Al-Refaie, A. F., Tennyson, J., & Yurchenko, S. N. 2014, MNRAS, 446, 2337
Stock, J. W., Kitzmann, D., & Patzer, A. B. C. 2022, MNRAS, 517, 4070
Stock, J. W., Kitzmann, D., Patzer, A. B. C., & Sedlmayr, E. 2018, MNRAS, 479, 865
STScI Development Team, 2013 pysynphot: Synthetic photometry software package, Astrophysics Source Code Library, ascl:1303.023
Taylor, J., Radica, M., Welbanks, L., et al. 2023, MNRAS, 524, 817
Tennyson, J., Yurchenko, S. N., Al-Refaie, A. F., et al. 2016, JMoSp, 327, 73
Tian, M., & Heng, K. 2024, ApJ, 963, 157
Trotta, R. 2008, ConPh, 49, 71
Tsai, S.-M., Innes, H., Wogan, N. F., & Schwieterman, E. W. 2024, ApJL, 966, L24
Tsai, S.-M., Lee, E. K. H., Powell, D., et al. 2023, Natur, 617, 483
Tsiaras, A., Waldmann, I. P., Zingales, T., et al. 2018, AJ, 155, 156
Underwood, D. S., Tennyson, J., Yurchenko, S. N., et al. 2016, MMNRAS, 459, 3890
Yang, J., Alday, J., & Irwin, P. 2024a, arXiv:2407.06932
Yang, J., Hammond, M., Piette, A. A. A., et al. 2024b, MNRAS, 532, 460
Yang, J., Irwin, P. G. J., & Barstow, J. K. 2023, MNRAS, 525, 5146
Yurchenko, S. N., Amundsen, D. S., Tennyson, J., & Waldmann, I. P. 2017, A&A, 605, A95
Yurchenko, S. N., Mellor, T. M., Freedman, R. S., & Tennyson, J. 2020, MNRAS, 496, 5282
Zhou, L., Ma, B., Wang, Y.-H., & Zhu, Y.-N. 2023, RAA, 23, 025011